J Mater Sci (2007) 42:2753–2757
DOI 10.1007/s10853-006-1272-4

Fabrication and optical property of single-crystalline InSb nanowire arrays

Youwen Yang · Liang Li · Xiaohu Huang · Guanghai Li · Lide Zhang

Received: 15 July 2005 / Accepted: 3 February 2006 / Published online: 9 January 2007

Abstract Semiconductor InSb nanowire arrays have been synthesized by the pulsed electrochemical deposition from citric acid aqueous solution into anodic alumina membranes. It was found that the InSb nanowires are of zinc-blende structure, and high filling rate and single-crystalline InSb nanowire array with right stoichiometric composition can be fabricated by proper controlling of the concentration of In and Sb ions and the PH value in the electrolyte and the pulse voltage, and the nanowires have [100] orientation with structure defects such as twins. The optical band gap has a strong blue shift with decreasing the diameter of the nanowire due to the quantum confinement effect.

Introduction

As a direct bandgap semiconductor, indium antimonide (InSb) has the smallest band gap, measuring 0.17 eV at 300 K and corresponding to IR wavelength (6.2 μm) [1]. It is an important semiconductor for use in electron and long wavelength optoelectronic device application. Because of its unique properties and potential application, InSb has attracted considerable attention in the last several years [2–4]. InSb quantum dots [5, 6], nanorods [7], and thin film [8–10] have been studied. However, the fabrication of InSb nanowires is still scarce.

Different methods are used to fabricate the nanowires, such as vapor–liquid–solid (VLS) [11], physical vapor deposition (PVD) [12], and hydrothermal [13]. Comparatively, the template synthesis method, using anodic alumina membranes (AAM), is effective and inexpensive method to fabricate nanowires [14]. Different materials, such as Bi, Si, Au, Ag, nanowires [15–18], TiO_2, Ag_2S, CdSe nanowires [19–21], and Bi_2Te_3 nanowire arrays [22] have been fabricated in AAM. The pulsed electrodeposition process is one of the most efficient methods for the growth of uniform and continuous nanowires [23–25].

In this paper, we report the fabrication and characterization of InSb nanowire arrays in AAM by the pulsed electrodeposition technique for the first time.

Experimental

The AAM templates were prepared by a two-step anodization process [23–25]. The high purity (99.999%) aluminum foils were degreased in acetone firstly, then annealed at 500 °C for 5 h and electropolished in a mixture of perchloric acid and ethanol (1:9) at 5 °C. The anodization was carried out at 40 V DC in 0.3 M oxalic acid aqueous solution at 7 °C. After first anodization for 4 h, the formed alumina was removed by a mixture solution of phosphoric and chromic acids for 6 h. Then the aluminum foil was anodized again for 16 h. The central remaining aluminum was removed in a saturated $SnCl_4$ solution, and the surrounding aluminum was retained as a support. Then the barrier layer was dissolved in 30 °C for

Y. Yang · L. Li · X. Huang · G. Li (✉) · L. Zhang
Key Laboratory of Materials Physics, Anhui Key Laboratory of Nanomaterials and Technology, Institute of Solid State Physics, Chinese Academy of Sciences, P.O. Box 1129, Hefei 230031, P. R. China
e-mail: ghli@issp.ac.cn

45 min. The pore diameter of the as-prepared AAM is about 60 nm. While the AAM with pore size of 80 nm is obtained by etching in H_3PO_4 solution at 30 °C for 40 min. Finally, a layer of Au film was sputtered onto one side of AAM to server as the working electrode.

The pulsed electrodeposition of the InSb nanowire arrays was performed in a two-electrode electrochemical cell controlled by computer, and a graphite plate was used as the counter electrode. The typical electrolyte solution contains 0.06 M $InCl_3{\cdot}4\ H_2O$, 0.045 M $SbCl_3$, 0.2 M $H_2C_6H_5O_7$ and 0.15 M $Na_3H_2C_6H_5O_7$. The PH value of the electrolyte was adjusted to 2.2 by HCl and the fabrication was performed at 20 °C at the voltage of –2.1 V.

The X-ray powder diffraction (XRD) spectrum of the nanowire arrays was obtained by an X-ray diffractometer (D/MAX-rA) with Cu Kα radiation (λ = 1.54178 Å). The structure was analyzed by field emission scanning electron microscope (FE-SEM) performed on JEOL JSM-6700F and a transmission electron microscope (TEM) on H-800. For the FE-SEM investigation, the sample was immersed in 5 wt% NaOH solution to partially remove the alumina template and then washed several times with deionized water. The TEM specimen was obtained by completely dissolving the AAM in 5 wt% NaOH solution and then rinsed with absolute ethanol and immersed in an ultrasonic bath for 8 min. High-resolution transmission electron microscopy (HRTEM, JEOL-2010) were used to study the crystalline structure and morphology of nanowires arrays. The chemical compositions of the nanowires were determined by energy dispersive spectrometer (EDS) attached in FE-SEM.

Results and discussion

The most important issue in fabricating InSb nanowires is to obtain right stoichiometric composition. We fixed the pulse frequency 1000 Hz ($t_{on} = t_{off}$ = 500 μs) and electrolysis temperature, and studied the influence of the relative concentration of In^{3+} and Sb^{3+} ions in the electrolyte, PH value of the electrolyte and the pulse voltage in the preparation of the nanowire arrays. The conditions are summarized in Table 1. Figure 1a shows a typical EDS pattern of the InSb nanowires deposited with the condition described in experimental section, which demonstrates that there are only In and Sb elements in the nanowires, the C and O peaks are due to the absorption, and the Cu peak is due to copper girding. Quantitative analysis indicates an atomic composition of 50.7% In and 49.3% Sb, which is very close to 1:1. The ratio of In to Sb in the nanowires almost linearly increases with increasing the PH value of the electrolyte, and at about 2.2 reaches about 1 when the $InCl_3/SbCl_3$ = 1.33 in the electrolyte at the pulse voltage of –2.1 V, see Fig. 1b. It is well known that to realize the co-deposition of In^{3+} and Sb^{3+}, a high concentration of the In^{3+} in the electrolyte is necessary in order to bring the electrode potentials of the In^{3+} closer to Sb^{3+}, because the electrode potential of In^{3+} is large than Sb^{3+}. We can see from the Fig. 1c that it is difficult to realize the co-deposition of In^{3+} and Sb^{3+} when $In^{3+}/Sb^{3+} < 1$ in the electrolyte, and only when the molar ratio of $InCl_3$ to $SbCl_3$ = 1.33 in the electrolyte that the atomic ratio of In to Sb in the InSb nanowires is about 1. The dependence of the ratio of In to Sb in the nanowire on the pulse voltage is nonlinear, and the In/Sb increases with the pulse voltage, and at about –2.1 V reaches about 1, and then increases again. From these results it was found that the InSb nanowires with high filling rate and right stoichiometric composition could be fabricated under the conditions of the pH = 2.2, voltage = –2.1 V and the molar ratio of $InCl_3/SbCl_3$ = 1.33 in the electrolyte. Under other deposition conditions, the resulting nanowires are admixture of In or Sb and InSb. It was also found the pulse frequency (100–1,600 Hz) is less important in determining the atomic ratio of In/Sb in the nanowires but plays a significant role in deciding the orientation of the nanowires.

Table 1 Deposition conditions for InSb nanowires

Condition	In^{3+}:Sb^{3+} (M)	Voltage (V)	PH value
1	4–0.7	–2.1	2.2
2	1.33	–1 to –2.5	2.2
3	1.33	–2.1	1.5–2.5

The XRD patterns of the InSb nanowire arrays pulsed electrodeposited with different conditions are shown in Fig. 2. One can see when the ratio of In^{3+}:Sb^{3+} = 2:3 (<1) in the electrolyte only Sb nanowires were obtained, See Fig. 2 curve a, and when the pulsed voltage increased to –2.4 V the admixture of In and InSb nanowires were formed, see Fig. 2 curve b with all other condition the same. Under the conditions of the pH = 2.2, voltage = –2.1 V and the molar ratio of $InCl_3/SbCl_3$ = 1.33 in the electrolyte, the diffraction peaks of the InSb nanowires fabricated can be index to a cubic zinc-blende phase of InSb crystal (JCPDS 060208), see Fig. 2 curve c, no other diffraction peaks, such as Sb and In, were observed indicating the pure InSb phase was fabricated. One also can see that the intensity of the diffraction peak at $2\theta = 56.6^{o}$ is relative strong than other diffraction peaks, demonstrating that

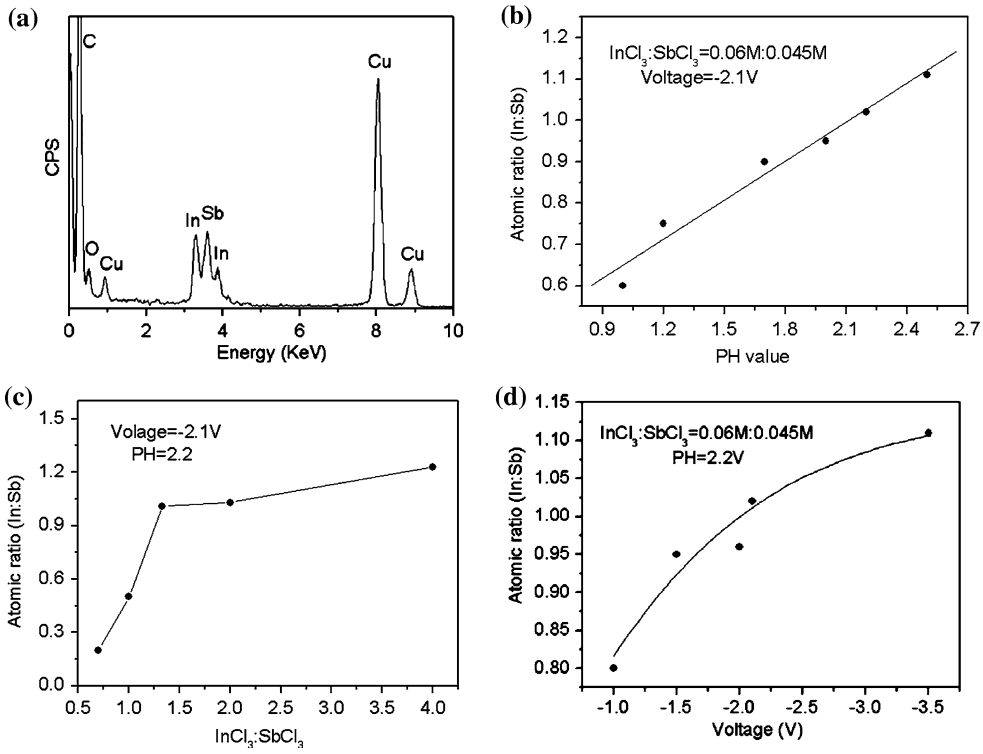

Fig. 1 (**a**) Typical EDS patters of InSb nanowires and the ratio of In:Sb in InSb nanowires as a function of (**b**) PH value, (**c**) In^{3+}:Sb^{3+} ratio in the electrolyte and (**d**) the pulse voltage

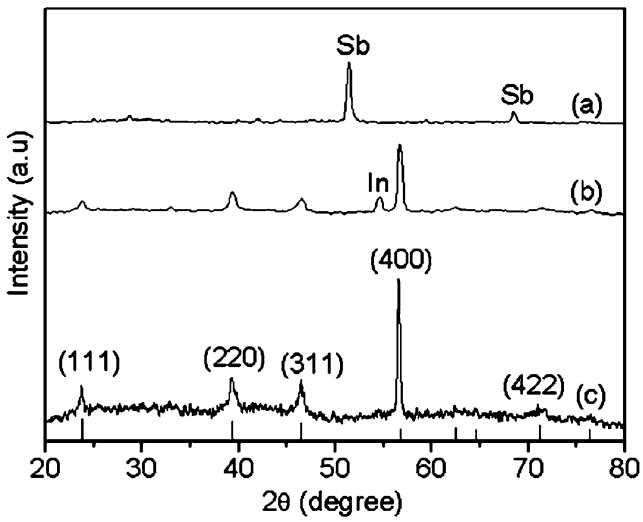

Fig. 2 XRD patters of InSb nanowires pulsed electrodeposition with the conditions of (**a**) $InCl_3/SbCl_3$ = 2:3, voltage = –2.1 V, (**b**) $InCl_3/SbCl_3$ = 1.33, voltage = –2.4 V and (**c**) $InCl_3/SbCl_3$ = 1.33, voltage = –2.1 V together with that from InSb crystal (JCPDS 060208)

the InSb nanowires deposited in AAM grow preferentially along [100] crystal direction.

Figure 3 shows the FE-SEM images of the InSb nanowire array after the AAM has been partly etched away for different times. One can see that almost all the pores are filled with InSb nanowires. The cross-section view of the nanowire array in Fig. 3c clearly indicates that the nanowires are parallel to each other with the length of about 60 μm, and uniformly distributed in the pores of AAM.

Figure 4 shows the TEM images of the InSb nanowires with diameter of 60 nm and 80 nm after the AAM was completely removed. The diameter of the nanowires is apparently consistent with the pore size of the AAM used. A typical TEM image of a single InSb nanowire with diameter of 60 nm is shown in Fig. 5 together with the corresponding diffraction pattern. The diffraction spots of (200), (11 $\bar{1}$) and ($\bar{1}$1 $\bar{1}$) lattice planes correspond to a single-crystal cubic zinc-blende structure of InSb (the inset in Fig. 5a). Calculation indicates that the incident beam is parallel to [011] direction. The HRTEM images in Fig. 5b and c are recorded from different areas of the nanowire, as marked in Fig. 5a, to reveal the local structures. It can be seen from Fig. 5b that the (200), (11 $\bar{1}$) and ($\bar{1}$1 $\bar{1}$) lattice fringes with lattice spacing about respectively 0.32, 0.380 and 0.38 nm show the two dimensional lattice planes. The (200) lattice fringes is perpendicular to the axis of the nanowire, indicating the growth direction of the InSb nanowires is along [100] direction, which is in consistent with the result of the X-ray diffraction. From the diffraction pattern one also can see that there are some twins or stacking faults in the nanowires and these planar

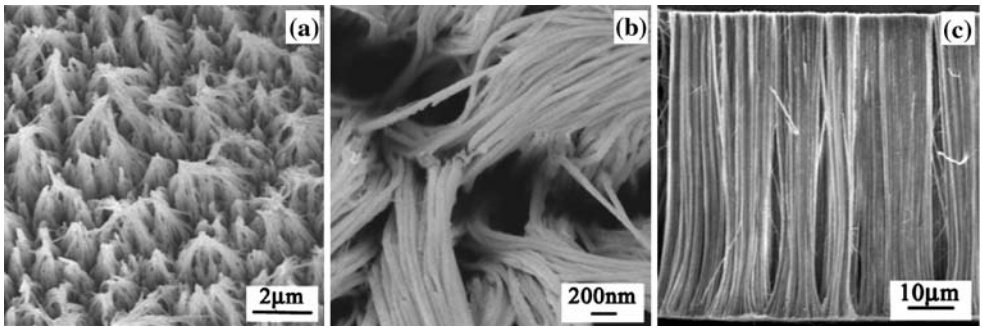

Fig. 3 FE-SEM images of the InSb nanowire array with diameter of 60 nm after the anodic alumina membranes (AAM) has been partly etched away for (**a**) 5 min and (**b**) 8 min, (**c**) cross-section view of the AAM filled with nanowires

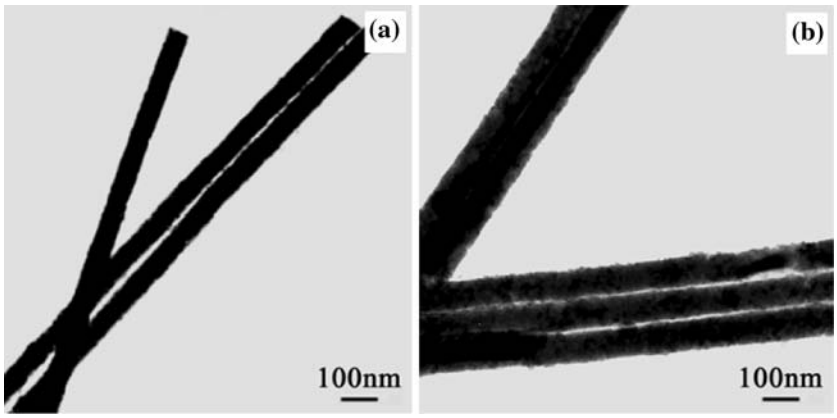

Fig. 4 TEM image of InSb nanowires with diameter of (**a**) 60 nm and (**b**) 80 nm

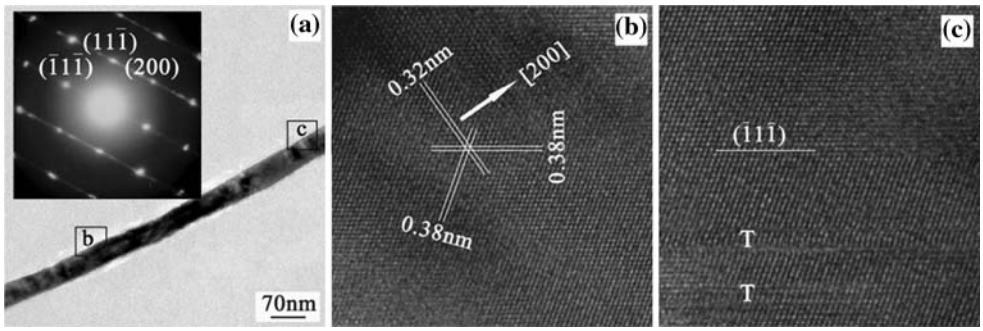

Fig. 5 Typical TEM image of (**a**) a single InSb nanowires with diameter of 60 nm, (**b**) and (**c**) HRTEM images of area marked in (**a**). The inset in (**a**) is the corresponding SAED pattern and the letters T in (**c**) is the indication of the twin structure

defect structures are in ($\bar{1}1$ $\bar{1}$) planes, as can be clearly seen in Fig. 5c. In cubic zinc-blende crystals twinning along the [111] direction is a well-known effect creating domains in which the main crystal axis orientation changes from domain to domain [26]. The planar defect structures might be caused by the fluctuation of system energy, which has a close relation with the surface and interface of the nanowires. Instability of the system energy will introduce strain and defects during crystal growth and lead to the formation of twins or stacking faults on the {111} facets. It was also found in our experimental that the InSb nanowire arrays with the diameter less than 60 nm are polycrystalline with nonstoichiometric composition.

Figure 6 shows the infrared absorption spectra of the InSb nanowire arrays with different diameters. One can see that the optical absorption edge moves to short wavelength region with decreasing the diameter. For the direct bandgap semiconductor the absorption coefficient α is connected with the band–gap energy E_g by the equation:

$$(\alpha h\nu)^2 = A(h\nu - E_g)$$

The inset in Fig. 6 shows the variation of $(\alpha h\nu)^2$ versus $h\nu$, and the energy gap is obtained by extrapolating the linear portion of the $(\alpha h\nu)^2$ versus $h\nu$ plot to $\alpha = 0$ (for α large than 10^4 cm^{-1}). The band gap energy is found to be about 1.70 eV for the 80 nm InSb

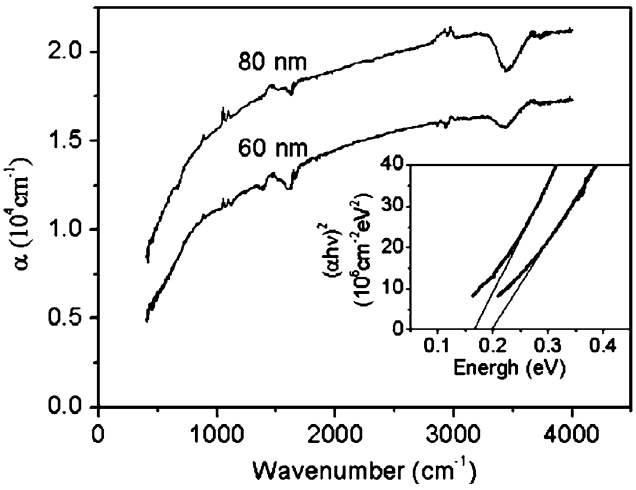

Fig. 6 Infrared absorption spectra of InSb nanowires with different diameters. The inset is the plot of $(\alpha h\nu)^2$ vs. $h\nu$

nanowire, which is coincident with the literature data for bulk InSb. However, the band gap moves to about 2.0 eV for 60 nm InSb nanowires, a very strong blue shift occurs. The exciton Bohr radius of InSb is about 65.5 nm [27], and the quantum confinement effect will dominate when the diameter of the InSb nanowires is less than its Bohr radius. Thus the strong blue shift of the optical band gap for 60 nm InSb nanowires is considered due to the quantum confinement effect.

Conclusion

In summary, we have successfully produced the highly ordered single crystalline InSb nanowires array in porous anodic alumina membrane by the pulsed electrodeposition. The results indicate that the nanowires have a zinc-blende single crystalline structure with twins or stacking faults on the {111} facets and grow along [100] direction. The proper controlling of the concentration of In and Sb ions and the PH value in the electrolyte and the pulse voltage is essential in fabricating the InSb nanowires with high filling rate and right stoichiometric composition. The optical band gap has a strong blue shift with decreasing the diameter of the nanowire due to the quantum confinement effect. And yet, it will be very interesting to study electrical transport properties of the InSb nanowires. Further work is underway.

Acknowledgements This work was supported by the National Natural Science Foundation of China (No:10474098) and in part by the Science & Reach Foundation of HFUT (No:040003F).

References

1. Xu DS, Xu YJ, Chen DP, Guo GL, Gui L, Tang YQ (2000) Adv Mater 12:520
2. Massidda S, Continenza A, Freeman AJ, De Pascale TM, Meloni F, Serra M (1990) Phys Rev B 41:12079
3. Petrzhik EA, Darinskaya EV, Erofeeva SA, Raukhman MR (2003) Phys Sol Stat 45:266
4. Kamilov IK, Stepurenko AA, Kovalev AS (1998) Phys Stat Sol (b) 209:395
5. Child RA, Nicholas RJ, Mason NJ, Shields P, Wells JPR, Bradley IV, Phillips J, Murdin BN (2004) Physica E 22:598
6. Nicholas RJ, Shields PA, Child RA, Li LJ, Alphandery E, Maxon NJ, Bumgy C (2004) Physica E 20:204
7. Yousuf M, Qadri SB, Skelton F (2003) Appl Phys A76:33
8. Fluop T, Bekele C, Landau U, Angus J, Kash K (2004) Thin solid Film 449:1
9. Mcchesney JJ, Haigh J, Dharmadasa IM, Mowthorpe DJ (1996) Optical Maters 6:63
10. Mengoli G, Mmusiani M, Paolucci F, Gazzano M (1991) J Appl Electrochem 21:863
11. Stach EA, Pauzauskie PJ, Kuykendall T, Goldberger J, He RR, Yang PD (2003) Nano Letts 3:867
12. Hulteen JC, Treichel DA, Smith MT, Duval ML, Jenson TR, Van DRP (1999) J Phys Chem B 103:3818
13. Wang X, Li YD (2002) J Am Chem Soc 124:2880
14. Banerjee S, Dan A, Chakravorty D (2002) J Mater Sci 37:4261
15. Li L, Zhang Y, Li GH, Song WH, Zhang LD (2005) Appl Phys A 80:1053
16. Lew KK, Redwing JM (2003) J Crys Growth 254:14
17. Sun X, Xu FQ, Li ZM, Zhang WH (2005) Maters Chem Phys 90:69
18. Zhang JX, Shi GQ, Liu C, Qu LT, Fu MX, Chen FE (2003) J Mater Sci 38:2423
19. Liu SQ, Huang K (2005) Solar Energy Maters Solar Cells 85:125
20. Gate B, Wu YY, Yin YD, Yang PD, Xia YN (2001) J Am Chem Soc 123:11500
21. Xu DS, Shi XS, Guo GL, Gui LL, Tang YQ (2000) J Phys Chem B 104:5061
22. Sander MS, Prieto AL, Grosky R, Sands T, Stacy AM (2002) Adv Mater 14:665
23. Zhang Y, Li GH, Wu YC, Zhang B, Song WH, Zhang LD (2002) Adv Mater 14:1227
24. Li L, Zhang Y, Li GH, Zhang LD (2003) Chem Phys Lett 378:244
25. Li L, Li GH, Zhang Y, Yang YW, Zhang LD (2004) J Phys Chem B 108:19380
26. Ohkawa K, Karasawa T, Mitsuyu T (1991) J Vac Sci Technol B 9:1934
27. Lin MC, Chen PY, Su IW (2001) J Electro Soc 10:c653